Applied Composite Materials (2022) 29:2125–2145
https://doi.org/10.1007/s10443-022-10056-x

Multiscale Simulation and Experimental Study of Metal Flow Behaviors in 3D Orthogonal Woven Fabric/Al Composites During Liquid Infiltration Process

Shouyin Zhang[1] · Xiating Li[1] · Zhenjun Wang[1] · Zhifeng Xu[1]

Received: 22 March 2022 / Accepted: 23 July 2022 / Published online: 17 August 2022

Abstract
In this paper, a novel aluminum matrix composites reinforced with 3D orthogonal woven fabric/ Al composite (3DOW/Al) is fabricated by gas pressure assisted liquid infiltration (GPI) method. The metal flow behaviors of inter-yarns and intra-yarn are investigated by multiscale simulations and experiments. The infiltration pressure and preheat temperature are the critical processing parameters in the forming of continuous carbon fiber-reinforced aluminum composites (CF/Al) composites. The threshold infiltration pressure is around 3 MPa, while the preheat temperature of fabric should be above the solidus of the matrix. The melt penetrates the interstices among yarns firstly due to the less flow resistance, then the internal fiber interstices in the yarns are filled gradually. The forming mechanism of microscopic intra-yarn voids and mesoscopic inter-yarns defects are clarified by the simulation in the mesoscopic and microscopic scale.

Keywords Aluminum matrix composite · 3D orthogonal woven fabric · Flow behavior · Liquid infiltration · Void defect

1 Introduction

Fiber-reinforced composites are gaining wide acceptance in many industrial applications. Fiber-reinforced composites based on thermoplastic matrix systems exhibit a high application potential for lightweight structures [1]. Metal matrix composites (MMCs) have some advantages compared to polymer matrix composites (PMCs), including higher matrix dependent strengths and moduli, higher elevated temperature resistance, higher electrical and thermal conductivities [2]. For instance, continuous carbon fiber-reinforced aluminum composites (CF/Al composites) exhibit significant improvements in specific strength, stiffness, and thermostability, etc. [3, 4], are of great potential in aerospace and automotive applications [4, 5]. Liquid metal infiltration processing is considered as an affordable technique to manufacture high quality CF/Al composites [3], where molten metal was

✉ Shouyin Zhang
zhangsy@nchu.edu.cn

[1] School of Aeronautic Manufacturing Engineering, Nanchang Hangkong University, Nanchang 330063, China

infiltrated into the preform under certain pressure [6]. It can be used to fabricate complex products with different kinds of fiber woven structures. However, most inorganic fibers such as carbon fiber, silicon carbide fiber and alumina fiber are not easily wetted by the molten metal due to their large contact angle [7, 8]. The poor wettability prevents the introduction of molten metal into fiber preforms. As Hajjari et al. reported, non-wettability problem as well as chemical reactions between melt and fibers are the main impediments to fabricate these high performance composites [4]. Closely packed fiber bundles may also cause poor infiltration and create defects in the composites. The solution of this problem is possible by applying external pressure to the melt that compensates the reverse capillary effect in the absence of wetting [5], as well as shorten the contact time between melt and fibers, which will reduce the interface reactions.

In fabrication of CF/Al composites by using gas pressure infiltration method, the pressure must exceed a “threshold pressure” [7, 9] which depends primarily on the fiber volume fraction, the fiber diameter, the preform architecture as well as the metal and preform temperature. Excessive pressure will drive the melt infiltrate into the graphite mold, resulting in the deterioration of the surface quality of composites. Therefore, certain high pressure up to several MPa should be applied to obtain the CF/Al composites part with high performance. The improved understanding of the infiltration of preforms should lead to the development of tailorable composite materials.

With liquid metal infiltration method, the flow behaviors of melt play a fundamental role in the fabrication of CF/Al composites. In order to achieve complete infiltration, an order of 10 or 100 MPa is required to drive the molten metal matrix into the preform [8]. Galyshev et al. investigated the relationship between infiltration pressure and the volume of voids fraction and found that the minimum pressure for complete infiltration of the carbon fibers was 12 MPa [5]. Lee and Hong studied the pressure infiltration casting process of high volume fraction (50-70 vol. %) SiCp/Al metal matrix composites and found that the required infiltration pressure was in the range of 10~50 MPa [10]. Hajjari et al. demonstrated that the appropriate applied pressure 30 MPa led to a good wettability and complete infiltration [4]. While a higher infiltration pressure (50-70 MPa) can cause the separation of coating on the carbon fibers.

From the above literatures, it can be found that a large range of infiltration pressure were applied to prepare the CF/Al composites. The parameters of fabrication process were usually set by trial and error approach, which was time consuming and expensive. Generally speaking, the utilization of the CF/Al composites is strongly inhibited by a lack of calculation methods, design principles and processes suitable for serial production [11]. Among this, the analysis of flow during the composites manufacturing process is a key step to process optimization. A good understanding of the filling process, as well as the flow behaviors both in macroscopic and microscopic scale are required to obtain CF/Al composites with high-quality.

The numerical simulations make it possible to optimize the injection process or to contribute to the design of the moulds both in the manufacturing process of polymer matrix composites (PMCs) and metal matrix composites (MMCs) [12]. The fibrous preform is assimilated to a porous medium, while the fluid is supposed to be incompressible. The flow is treated as a problem of fluid mechanics in a porous medium.

Permeability, which is represented in terms of fiber volume fraction, is a key parameter to determine the resin velocity. In many cases, the structure of fiber reinforcement is highly heterogeneous. Hence the permeability of preform presents anisotropy. The characterization of these textile fabrics depends on the observation scale. Researchers have attempted to simulate the resin flow behaviors in different scales [13–15]. In general, it is a customary approach to model the resin flow in the fiber reinforcement by Darcy's law in the macroscopic scale, aim to optimize the mold design and infiltration process. Gauvin et al. [16] investigated the flow of resin through the reinforcement in resin transfer molding (RTM) by using RTMFLOT software. Macroscopic flow field was obtained by assuming that the fabric is isotropic. Flow analysis at the mesoscale is applied to evaluate the preform permeability. While the modeling of the resin flow between the fiber filaments at the microscopic scale by Stokes' flow equation is used to explain the void formation mechanism inside the fiber tow.

Michaud et al. [8] summarized the infiltration processing of fiber reinforced composites and found that the governing of all three classes of fiber reinforced composite materials (polymer matrix, metal matrix, ceramic matrix) are essentially the same. However, phenomena such as phase change, segregation and microporosities formation are involved in the MMCs processing. These phenomena are more complex than the PMCs manufacturing, and need to be taken into account in the numerical simulation of flow analysis [12].

Previous studied have explored the infiltration process in different scale in the manufacturing of the PMCs. However, in the case of MMCs, most researchers investigated the flow behaviors in the fiber scale. Dopler et al. [17] developed a finite element model to simulate the metal infiltration of a rigid fibrous preform by taking into account capillary phenomena. Results showed that the value of specific permeability had a strong impact on the front kinetics, but exerted a weak influence on the shape of the saturation profile. Mantaux et al. [18] described the appearance of microporosites during the solidification of a pure metal within a fibrous preform. However, there are relatively few studies in the area of the forming process in the fabricating process of MMCs. Meanwhile, the infiltration behaviors in different scales need to be further clarified.

In this study, numerical simulations will be implemented to investigate the forming process and the flow behaviors of melt in the preparation of 3D orthogonal woven fabric/ Al composite (3DOW/Al). Experiments will be conducted to verify the numerical simulation. The aim of this work is to enhance the understanding of infiltrating phenomena in macroscopic, mesoscopic and microscopic scale, as well as to clarify the appropriate infiltration pressure in the preparing of 3DOW/Al composite.

2 Materials and Methods

Gas pressure assisted liquid infiltration (GPI) process, as one kind of liquid metal infiltration method, was used to synthesizing a T-shaped 3DOW/Al composite part. Previous research has shown that the wettability between the carbon fiber and melt can be improved by increasing magnesium content [19]. Therefore, ZL301 alloy with high content of magnesium (up to 9.5~11.0 wt. %) will be used as the matrix material. The chemical compositions of ZL301 alloy are given in Table 1. The CF/Al composite will eventually be used to manufacture stator blades. Therefore, a T-shaped sample (Fig. 1a) similar to the stator blade was designed and produced by using the GPI process in this study. Vibration characteristics will be tested in further research. Figure 1b presents 3-D orthogonal woven fabric which was woven by graphite fiber M40J. The nominal properties of graphite fiber M40J provided by the manufacturer are

Table 1 Chemical compositions of ZL301 alloy (wt. %)

Element	Mg	Si	Cu	Mn	Ti	Al
Concentration	9.5-11.0	0.3	0.1	0.15	0.15	Balance

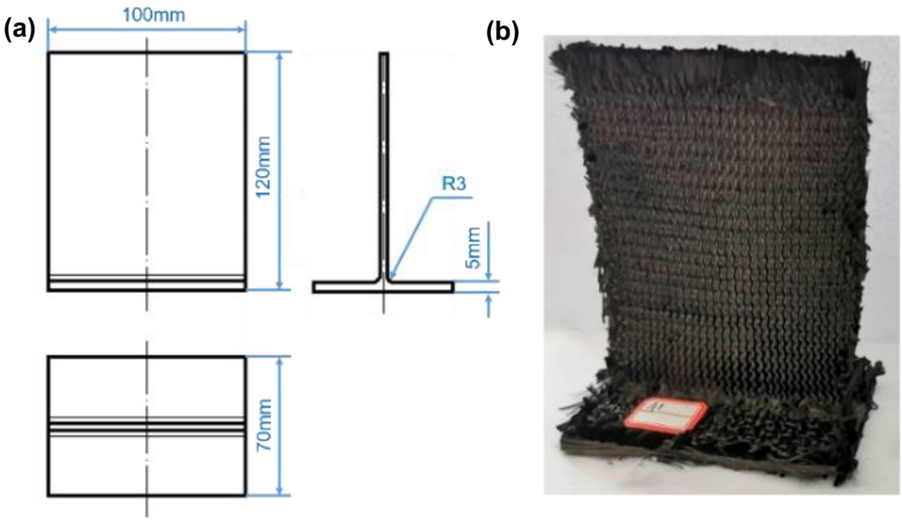

Fig. 1 **a** Two-dimensional graph of T-shaped CF/Al composite part; **b** Appearance of 3-D orthogonal woven fabric

shown in Table 2. Figure 2 presents the structure model of the 3DOW/Al composite. Primary properties of the graphite fiber M40J and architecture parameters of the 3D orthogonal woven fabric can be found in Tables 3 and 4, respectively. The prepared fabric will be assembled into the graphite mold, and then sealed with stainless steel sheet. The assembled mold will be put into the gas pressure assisted infiltration furnace. Then the mold will be heated to the preheat temperature with a heating rate 10 ℃/min and held for 30 min. Schematic diagram and physical drawing of the GPI apparatus are presented in Fig. 3. In the fabricating process, the cavity of the furnace including the mold will be vacuumed to a pressure below 1 Pa. Then the compressed inert Ar gas will be used to provide the required pressure for infiltration. With the pressure exerted on the surface of melt (ZL301 alloy), melt will rise through lift tube and infiltrate into the fabric. After complete solidification, T-shaped 3DOW/Al composite part will be fabricated.

3 Numerical Simulations

3.1 Theory

It is a customary approach to model the resin flow [20] in the fiber reinforcement of PMCs and metal flow in the fiber reinforcement of MMCs [18] by Darcy's law. Darcy's law depicts fluid flow behaviors in porous media. The one-dimensional Darcy equation can be written as [21]:

Table 2 Primary properties of the graphite fiber M40J

Properties	E/GPa	σ_b/MPa	ρ/g·cm^{-3}	Ductility/%	Diameter/μm
M40J	377	4400	1.81	0.7	6

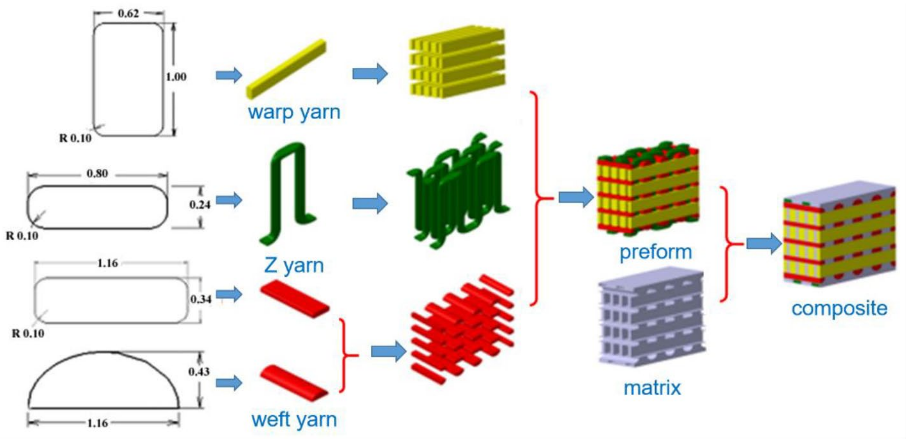

Fig. 2 Structure model of the 3DOW/Al composite

$$-\frac{\mathrm{d}p}{\mathrm{d}X}=\frac{\mu v}{k} \tag{1}$$

where p is the pressure, X is the direction of fluid flow, μ is the viscosity, v is the superficial velocity, and k is the permeability. In the equation, the pressure gradient is linearly proportional to the fluid velocity in the porous media. However, several works indicated that Darcy' law is valid under a limited range of low velocities owing to fluid inertia [16, 22]. The relationship between flow rate and pressure gradient becomes non-linear at sufficiently high velocity [21]. Therefore, many researchers attempted to correct this equation in order to describe the non-Darcy flow in porous media. Forchheimer [23] attributed the deviation from linearity to the microscopic inertial effect, and corrected the Darcy equation as follow:

$$-\frac{\mathrm{d}p}{\mathrm{d}X}=\frac{\mu v}{k}+\beta\rho v^2 \tag{2}$$

where β is the non-Darcy coefficient to describe the increasing contribution to pressure drop caused by inertial losses, ρ is the fluid density.

As discussed above, a high pressure is required to obtain a sound CF/Al composites part. However, it is difficult to identify the critical point for the initiation of non-Darcy behavior, which is usually not accurate and less dependable [24]. Therefore, a

Table 3 Architecture parameters of the 3D orthogonal woven fabric

Fabric structure	Fabric size(mm)	Yarn density(bundle/cm)	Yarn specification	Fabric weight(kg)	Fiber content(%)
3D orthogonal	120×100×70	Warp: 12 Weft: 5	Warp yarn: M40 6K×3 Weft yarn: M40 6K×2 Z yarn: M40 6K×1	0.975	50

Table 4 Input parameters of numerical simulation

Input parameters	Variable	Value
Liquidus temperature (ZL301)	T_L	607 ℃
Solidus temperature (ZL301)	T_S	504 ℃
Surface tension (molten ZL301)	σ	0.87 N/m
Conductivity (MJ40 fiber)		68.67 W/(m K)
Heat transfer coefficient (metal and MJ40 fiber)		1000 W/(m^2·K)
Specific heat (MJ40 fiber)		711.76 J/kg/K
Heat transfer coefficient (mold and casting)		Ref. 28 (Figure 7)
Heat transfer coefficient (air and mold)		10 W/(m^2·K)
Surface area per unit volume (MJ40 fiber)	S_a	5500 1/cm
Void fraction of fabric	V_a	0.48
Void fraction of yarn	V_a	0.7

convenient method by determining the permeability of filter based upon Carman-Kozeny theory was applied. The permeability of the fabric and yarn, i.e. its resistance to the flow, can be calculated according to the following relationship [25]:

$$K = \frac{{F_v}^3}{5{S_a}^2(1 - F_v)^2} \tag{3}$$

where F_v is the void fraction of the fabric, S_a is the surface area per unit volume.

The void fraction (F_v) corresponds to the amount of void inside the porous material. The surface area per unit volume (S_a) corresponds to the amount of "interface" between the porous material and the fluid per unit volume, as illustrated in Fig. 4 [26]. This value can be used for the calculation of the permeability. The units are the reversed of a distance (e.g. [1/cm]).

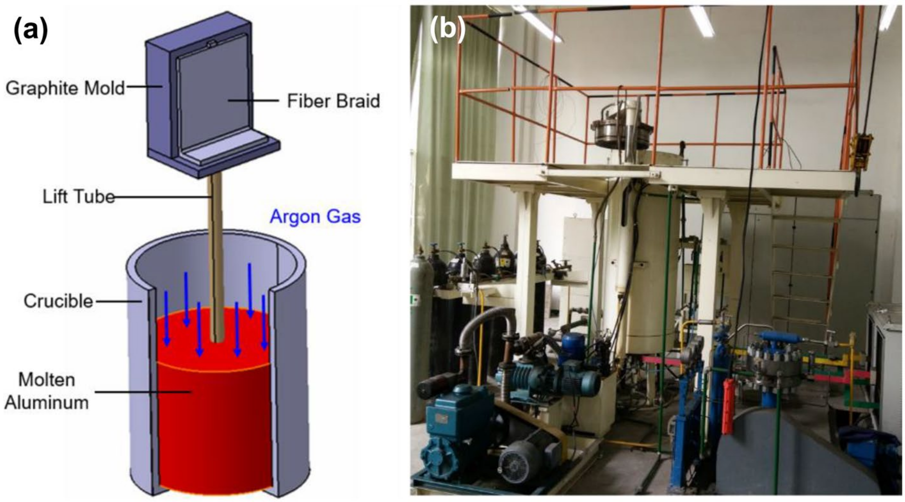

Fig. 3 Schematic diagram **a** and physical drawing **b** of the GPI apparatus

According to the back scattered SEM micrograph of 3DOW/Al composite (Fig. 8a), the surface area per unit volume is calculated as 5500 1/cm. The volume percentage of carbon fibers of the CF/Al composite is 52 % as tested, while the volume percentage of the matrix is 48%. Therefore, the void fraction of the fabric is 0.48. While for the yarns, the void fraction is 0.70 as calculated. These two values will be used in the simulation processes of macroscopic and mesoscopic flow, respectively.

3.2 Solution Methods

The microstructure of fiber reinforcement, in particular textile fabrics, is highly heterogeneous, and the characterization of these textile fabrics depends on the observation scale. From the macroscopic scale where the computational domain is greater than 0.1 m and the textile reinforcement can be observed by the naked eye, fiber reinforcement is usually considered as a homogenous porous medium [20]. Flow behaviors of melt in manufacturing the T-shaped CF/Al composite part can be classified as three scales, including the macroscopic flow in the graphite mold, the mesoscopic flow among the yarns, and the microscopic infiltration behavior inside the single yarn. In macroscopic scale, the size of computational domain is above 10 mm. The purpose of numerical simulation is mold design and process optimization. In mesoscopic scale, the size of computational domain is 1~10 mm. The purpose is understanding tow impregnation physic. While in microscopic scale, the size of computational domain is below 1 mm. The purpose is interpreting the infiltration behaviors among the fibers in the single yarn.

Flow behaviors are determined by the exerted pressure, the temperature of melt, the preheat temperature of mold and fabric, the structure and void fraction of fabric, as well as the thermophysical parameters of selected matrix material. In this paper, the macroscopic and mesoscopic flow behaviors are modelled by using the finite element (FEM) method under the ProCAST software. For macroscopic fluidity, T-shaped fabric can be considered as a homogenous filter material, while the parts of lift tube and vent are set as melt. The configuration and discretized mesh of the assembled graphite mold and T-shaped CF/Al composite part are showed in Fig. 5. The total tetrahedral mesh number is 557,000. More denser meshes were applied for the computation till the simulation results does not change with the size of the meshes.

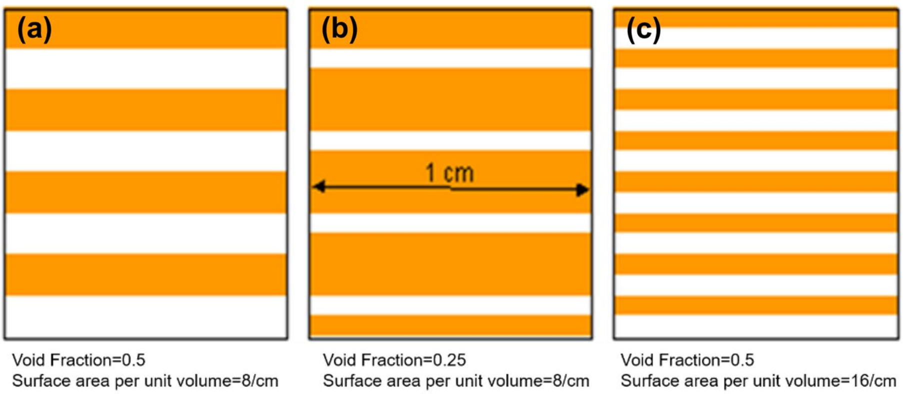

Fig.4 Definition of void fraction and surface areas per unit volume

Fig. 5 Discretized mesh of assembled graphite mold and T-shaped CF/Al composite part

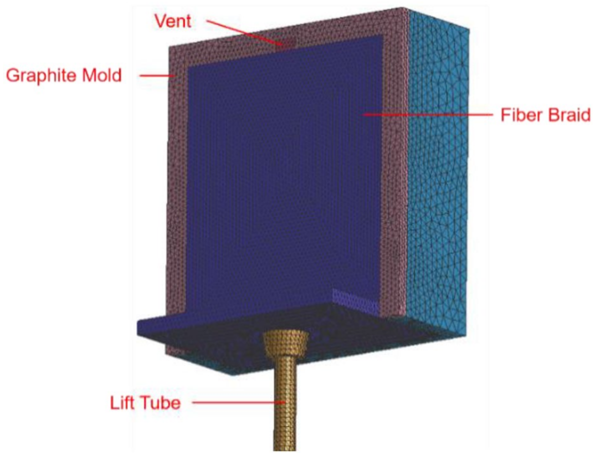

The fabric was set as filter material with S_a (the surface area per unit volume) 5500 1/cm, and with V_a (the void fraction) 0.48. The initial temperatures of graphite mold and fabric are set to 550 ℃. The pouring temperature is 720 ℃. In order to study the formability of the T-shaped CF/Al composite part, different infiltration pressures (0.05, 0.1, 0.5, 1, 3, 5, 7 MPa) are applied at the inlet, i.e., at the bottom of lift tube.

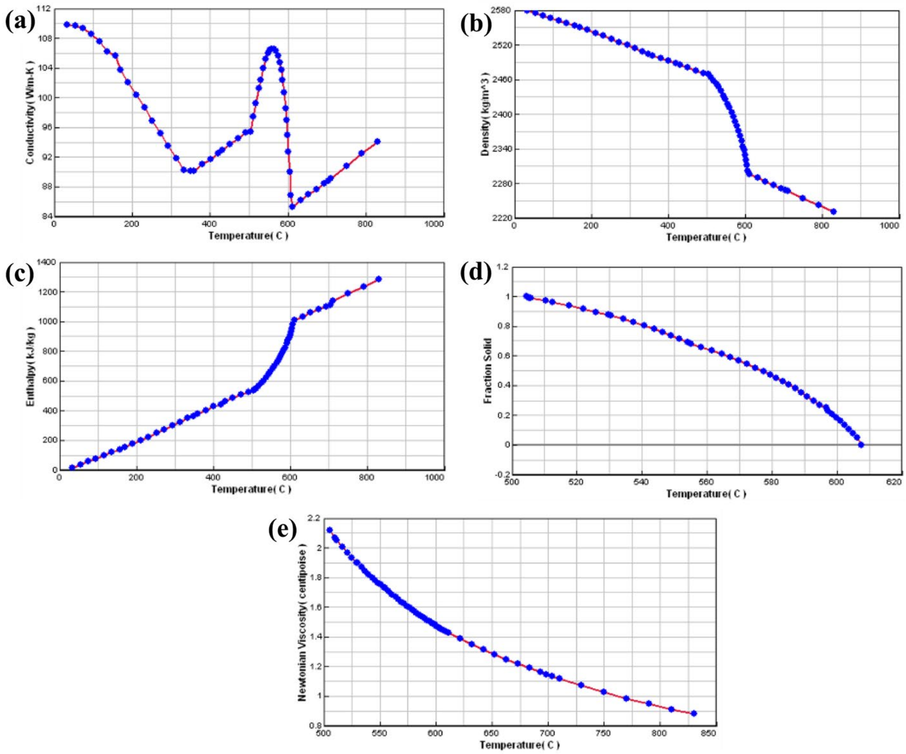

Fig. 6 Thermophysical parameters of ZL301 alloy: **a** conductivity; **b** density; **c** enthalpy; **d** fraction solid; **e** viscosity

Since the graphite mold is preheated to a certain high temperature, slow solidification process will be achieved in the infiltration process. Therefore, solid diffusion model "level rule", which corresponding to a complete mixing of the solute in solid, was selected to compute the thermophysical parameters of ZL301 alloy in ProCAST platform. The calculated liquidus and solidus are 607 ℃ and 504 ℃, respectively. The surface tension of molten ZL301 alloy is about 0.87 N/m [8]. Thermophysical parameters of ZL301 alloy are presented in Fig. 6.

As provided by the manufacturer, the conductivity of the graphite fiber M40J is 68.67 W/(m K). The specific heat is 711.76 J/kg/K. Heat transfer coefficient of interface between graphite mold and aluminum alloy was determined by Bazhenov et al. [27], as showed in Fig. 7. Heat transfer coefficient of filter, i.e., the interface between fibers and matrix (ZL301 alloy), was set to 1000 W/(m^2·K). Other input parameters of the numerical simulation are listed in Table 4.

The macroscopic flow simulation is based on the assumption that the fabric is isotropic. In order to study the effect of fabric structure on the flow behaviors of melt, a 3-D orthogonal structure RVE (representative volume element) that composes of yarns and matrix was built. The size of the RVE is 7.0 mm×3.6 mm×8.6 mm. The total tetrahedral mesh number is 2,146,000, as shown in Fig. 8. Mesoscopic flow simulation was implemented by using ProCAST platform. The 3-D orthogonal woven fabric is considered as the filter materials with S_a 5500 1/cm and with V_a 0.70. The initial temperature of fabric is 550 ℃, while the pouring temperature of melt is 720 ℃. Different infiltration pressures (10 kPa, 100 kPa, 1 MPa) are applied in the simulation.

Due to the dimension limitation, the simulation of microscopic infiltration process cannot be realized by using ProCAST software. Hence, a computational fluid dynamics (CFD) software FLUENT was utilized to study the infiltration behavior of melt in the yarns. In order to improve the accuracy of simulation, model was built according to the fiber arrangement in the previous SEM micrograph of CF/Al composites, as shown in Fig. 9a and b. The dimension of the model is 55 μm×55 μm×100 μm. The meshed

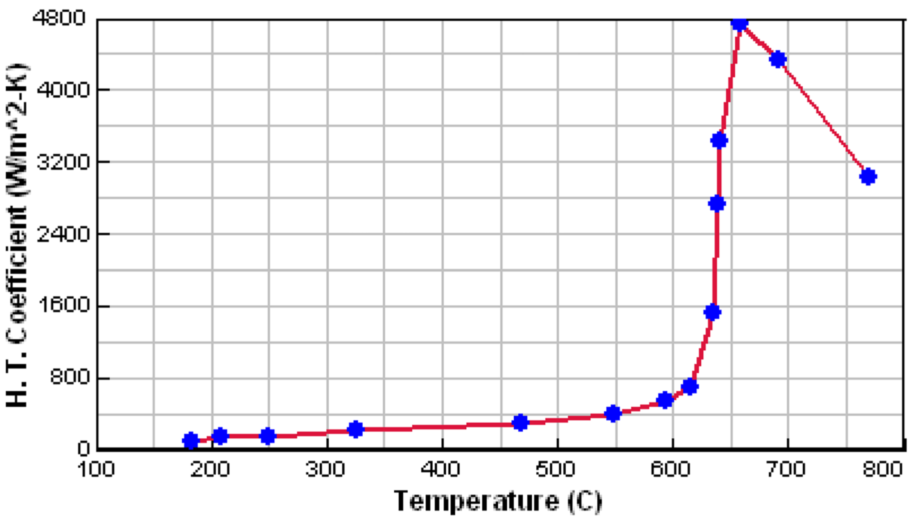

Fig. 7 Heat transfer coefficient of interface between graphite mold and aluminum alloy

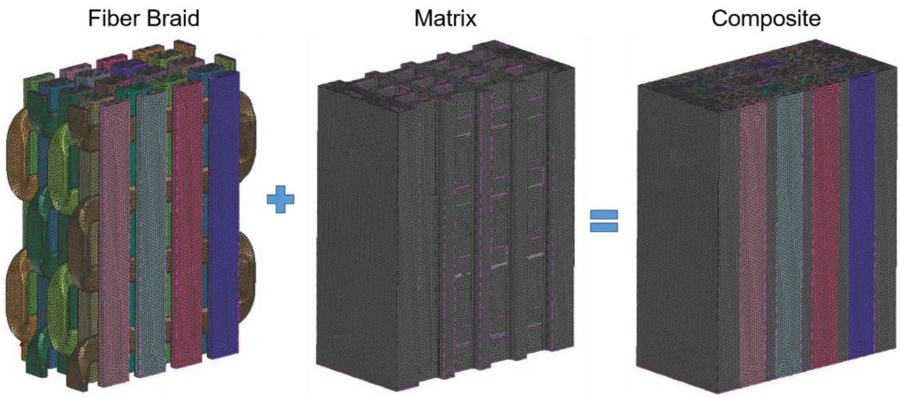

Fig. 8 FEM mesh of a 3-D orthogonal structure unit cell

model is presented in Fig. 9c. The inlet, outlet and symmetry boundaries are illustrated in Fig. 9c. New material (ZL301 alloy) with the thermophysical parameters (Fig. 6) is added to the database in FLUENT code. Multiphase VOF (volume of fraction), Energy equation as well as Solidification & Melting models are used in the simulation. The initial temperature of fiber and the melt are set to 550 ℃ and 720 ℃. The infiltration pressures used in the mesoscopic simulation (10 kPa, 100 kPa, 1 MPa) are selected to simulate the infiltration process in the yarns. The incompressible unsteady-state Navier-Stokes equations will be solved numerically to obtain the viscous flow fields.

4 Simulation Results

4.1 Macroscopic Flow Simulation

Fill percentage and fill time depending on infiltration pressure are illustrated in Fig. 10. It indicates that with higher applied infiltration pressure, less fill time is need in the infiltration process. T-shaped CF/Al composite part can be fully filled only when the pressure is greater than 3 MPa. With the applied infiltration pressure 3 MPa, 5 MPa, 7 MPa, the

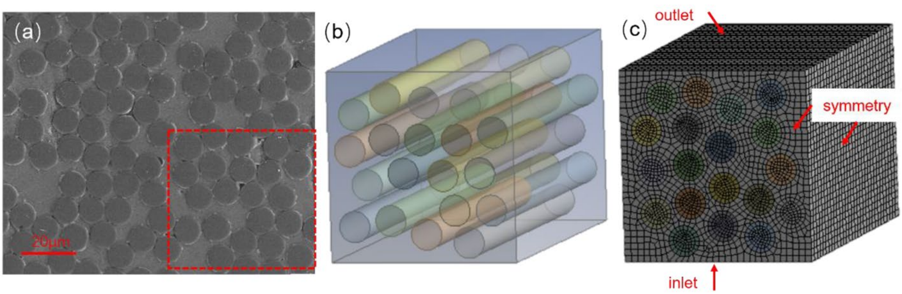

Fig. 9 **a** Back scattered SEM micrograph of CF/Al composites; **b** geometric model constructed according to the micrograph; **c** meshing

corresponding fill time are 4.2s, 2.5s and 1.8s, respectively. When the pressure is lower than 1 MPa, the fabric cannot be infiltrated completely. With lower infiltrating pressure, longer infiltration time is required. The melt loses its fluidity hence. It can be concluded that the threshold pressure for the manufacturing T-shaped CF/Al composite part is around 3 MPa. From the simulation results it can be found that there is no obvious difference of fill time with the fill percentage lower than 30%. This is due to the volume of melt in the lift tube accounts for 30%. After the lift tube is fully filled, melt begins to infiltrate into the fabric.

Based on the above analysis, it is recommend that the infiltration pressures applied should be greater than 3 MPa. However, in an actual experiment, it takes a certain amount of time to reach the specified pressure. Consequently, a higher pressure is required to achieve the completely infiltration. The actual curve of pressure with the maximum pressure 9 MPa was recorded as shown in Fig. 11. By using the actual pressure, simulation was performed with the preheat temperature 550 ℃ and with the pouring temperature 720 ℃. Fill percentage in the simulation is depicted in Fig. 11. Results show that T-shaped CF/Al composite part can be fully filled in 6.5s. With fill percentage of 100%, the infiltration pressure reaches 5.5 MPa approximately.

The preheat temperature of graphite mold and fabric plays a significant role in the fabrication of CF/Al composites part. Therefore, the formability of T-shaped CF/Al composite part was studied by using different preheat temperatures, 300 ℃, 450 ℃ and 550 ℃.

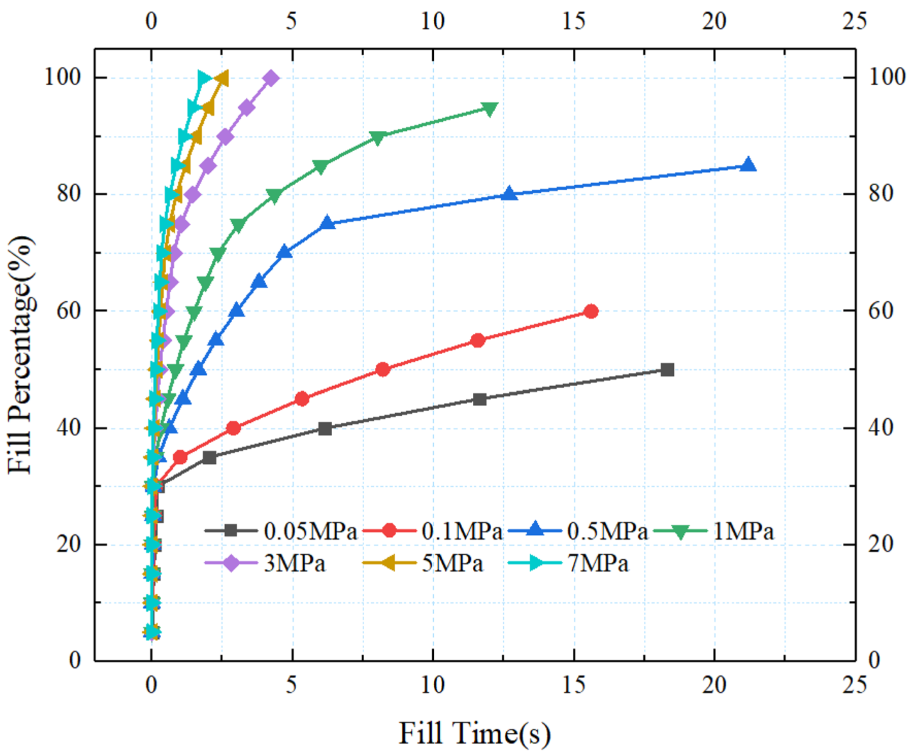

Fig. 10 Fill percentage and fill time depending on infiltration pressure

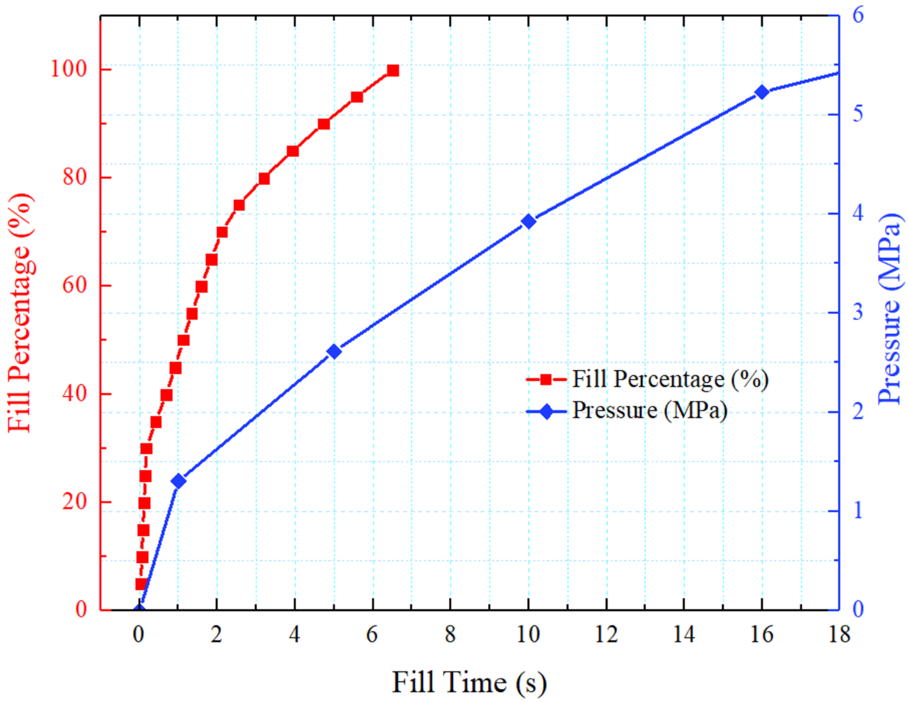

Fig. 11 Fill percentage and fill time depending on the actual applied pressure

Simulation results are presented in Fig. 12. With the preheat temperatures of 300 ℃ and 450 ℃, infiltration of melt cease at the fill percentage of 81% (Fig. 12d) and 89% (Fig. 12h), respectively. When the temperature of flow front decreases to the solidus, the viscosity of melt increases dramatically. Then the fill percentage will not increase significantly with the increasing fill time. When the preheat temperatures is set to 550 ℃, T-shaped CF/Al composite can be completely infiltrated at 6.7s. It can be observed that the vent on the top was fully filled as well (Fig. 12l).

In summary, with the preheat temperatures 550 ℃, which is above the solidus, complete infiltration can be achieved. It is noteworthy that the filling processes of melt in macroscale are relatively smooth regardless of the applied pressure and the preheated temperature.

4.2 Mesoscopic Flow Simulation

The simulated infiltration process of melt with a 3-D orthogonal woven structure are shown in Fig. 13. The results show that with higher pressure, less fill time is need to complete the infiltration process. Turbulence flows occur in the mesoscopic scale regardless of the infiltration pressure values. Melt fills the wider channels first, then the relatively narrower channels. Therefore, the fabric should adhere tightly to graphite mold to avoid a large clearance during assembly. In addition, uniform and dense fabric should be woven to ensure the smooth infiltration. Due to the high vacuum environment,

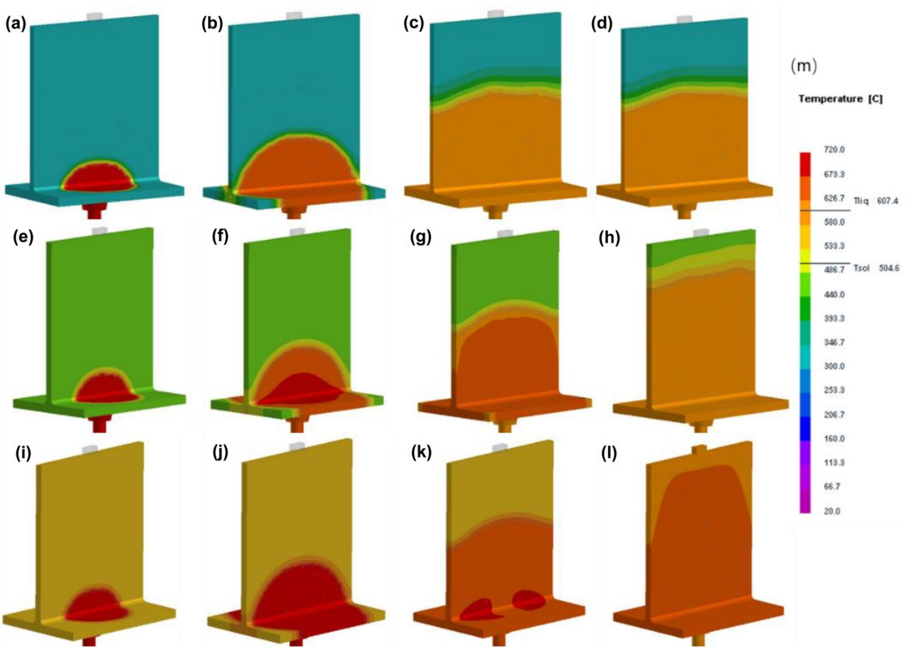

Fig. 12 Fill percentage and fill time with different preheat temperatures of mold and preform: **a**-**d**, 300 ℃, **a** 40%, 0.7s; **b** 60%, 1.6s; **a** 80%, 4.5s; **d** 81%, 5.0s; **e**-**h**, 450 ℃, **e** 40%, 0.7s; **f** 60%, 1.6s; **g** 80%, 3.3s; **h** 89%, 6.5s; **i**-**l**, 550 ℃, **i** 40%, 0.7s; **j** 60%, 1.6s; **k** 80%, 3.2s; **l** 100%, 6.7s; **m** thermal scale

as well as the high temperature of the melt and the fabric, no void will be introduced. Considering that the RVE was used in the mesoscopic flow simulation, it doesn't mean that the selected infiltration pressure are sufficient to fabricate the composite part.

The temperature of yarns with infiltration pressure 1 MPa (Fig. 13l) is lower than that the infiltration pressure 10 kPa (Fig. 13d) and 100 kPa (Fig. 13h) at the end of infiltration process. This can be attributed to the less infiltration time with high infiltration pressure.

Figure 14 presents the infiltrating behavior of inter-yarn with preheat temperature 300 ℃ and infiltration pressure 10 kPa. Partial yarns are displayed for comparison (Fig. 14a). It can be observed that with less flow resistance among the yarns, the melt penetrates the interstices of inter-yarn firstly. Then the melt infiltrates into the intra-yarn along its transverse direction as showed in the white box in Fig. 14a. As time progresses, the yarns are completely infiltrated (Fig. 14d). This phenomenon is consistent with the pressure assisted infiltration processing of metal matrix composites (MMCs) studied by Huchler [28], who summarized that there are two stages during infiltration, including flow initiation characterized by the dynamic wetting angle and the advancing flow in the preform capillaries.

It can also be noticed that the front melt cool fast with low preheat temperature and infiltration pressure. When the temperature drops to the solidus, the melt might cease to infiltrate further, which will result the void defects in the yarns.

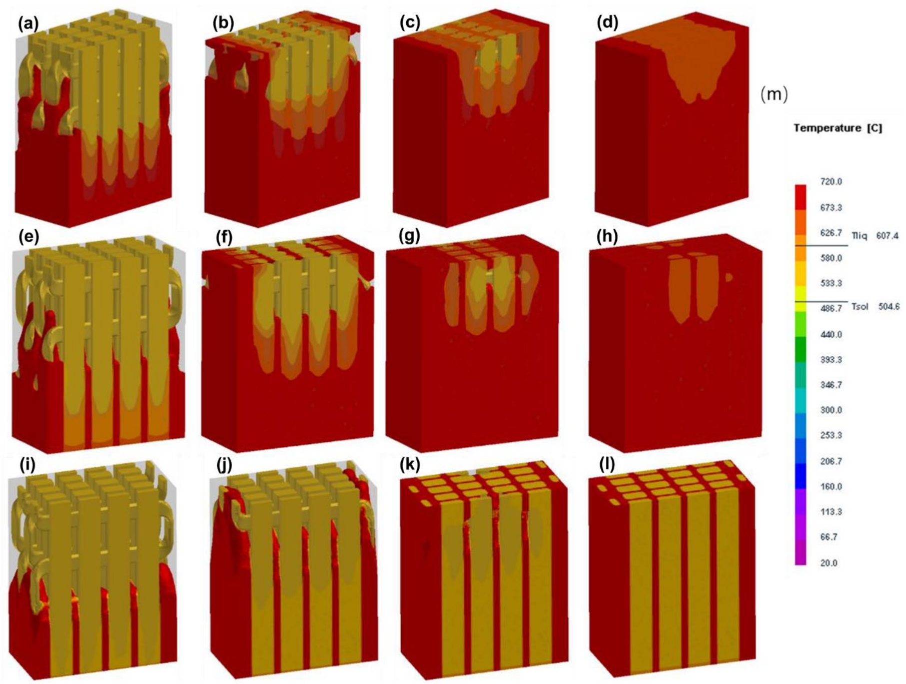

Fig. 13 Fill percentage and fill time with different infiltration pressure: **a**-**d**, 10 kPa, **a** 44%, 0.025s; **b** 73%, 0.0057s; **c** 90%, 0.0086s; **d** 100%, 0.01s; **e**-**h**, 100 kPa, **e** 41%, 0.0003s; **f** 77%, 0.0010s; **g** 95%, 0.0020s; **h** 100%, 0.0026s; **i**-**l**, 1 Mpa: **i** 40%, 0.0001s; **j** 72.5%, 0.0001s; **k** 91.6%, 0.0001s; **l** 100%, 0.0001s; **m** thermal scale

4.3 Microscopic Flow Simulation

It was reported that Al exhibits a non-wetting nature below 850 ℃ on most inorganic materials [29]. Candan et al. [30] investigated the effect of element Mg on the wettability of Al/SiC, and found that the wetting condition can be improved progressively by increasing the content of Mg. The wetting angle decreased from 120° (Pure Al) to 60° (Al-13.9Mg). This is the reason that the materials ZL301 alloy was selected as the matrix of composite in this study. Studied also showed that the contact angle decreased with the increased contact time. The increased

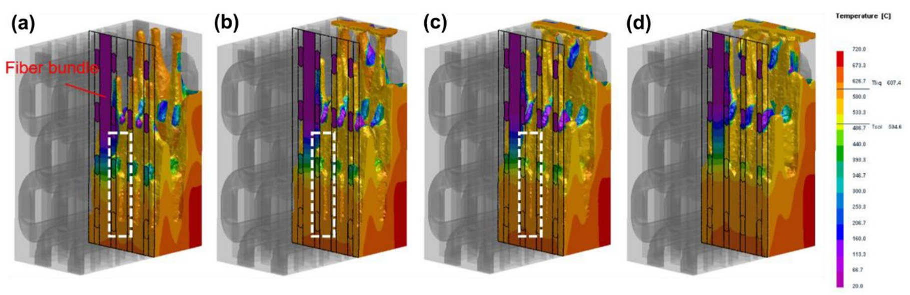

Fig. 14 Infiltrating behavior of melt in the fiber bundles with preheat temperature 300 ℃ and infiltration pressure 10 kPa

interfacial reaction leads to the reduced interface tension, resulting in the reduction of contact angle. Candan et al. [31] and Iseki et al. [32] reported that Al_4C_3 forms at the interface of Al/SiC composites. A block Al_4C_3 phase was found in the interface of the CF/Al composites in our previous research [33].

Capillary forces are of primary flow resistance in the infiltration process of MMCs [34]. The infiltration pressure should be larger than the capillary pressure (P_c) to circumvent the flow resistance. The value can be calculated by the Yong-Kelvin equation [35, 36]:

$$P_c = -\frac{4\gamma\cos\theta}{d} \tag{4}$$

where P_c (MPa) is capillary pressure difference, γ (N/m) is the surface tension of melt, θ denotes the wetting angle, and d (μm) is the capillary radius, i.e., effective diameter of the channel in the fiber bundles.

The surface tension of pure aluminum with substrate graphite in vacuum environment is 0.885 N/m as tested by Bainbridge et al. [37]. The surface tension of Al-0.26Si and Al-0.26Si-0.25Mg are 0.840 and 0.610 N/m, respectively. With higher Mg content (9.5-11.0 wt.% in ZL301 alloy), lower value can be expected. Wetting angle with high content Mg element (Al-8.6Mg) is about 60° [30]. The minimum capillary radius of intra-yarn is around 1μm as

Table 5 Flow morphology of intra-yarn with different infiltration pressure

Pressure \ Time	1E-06 s	1E-05 s	1E-04 s	5E-04 s
10kPa				
100kPa	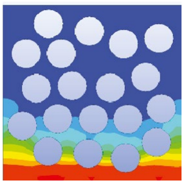	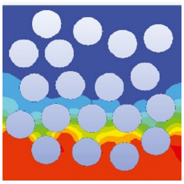	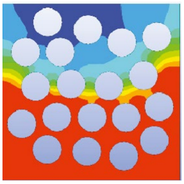	
500kPa	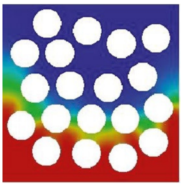	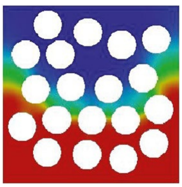	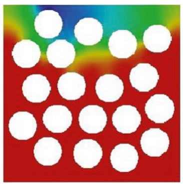	
1MPa	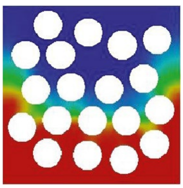	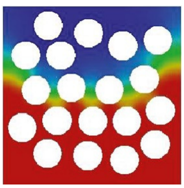	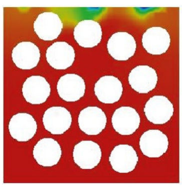	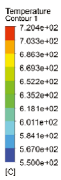

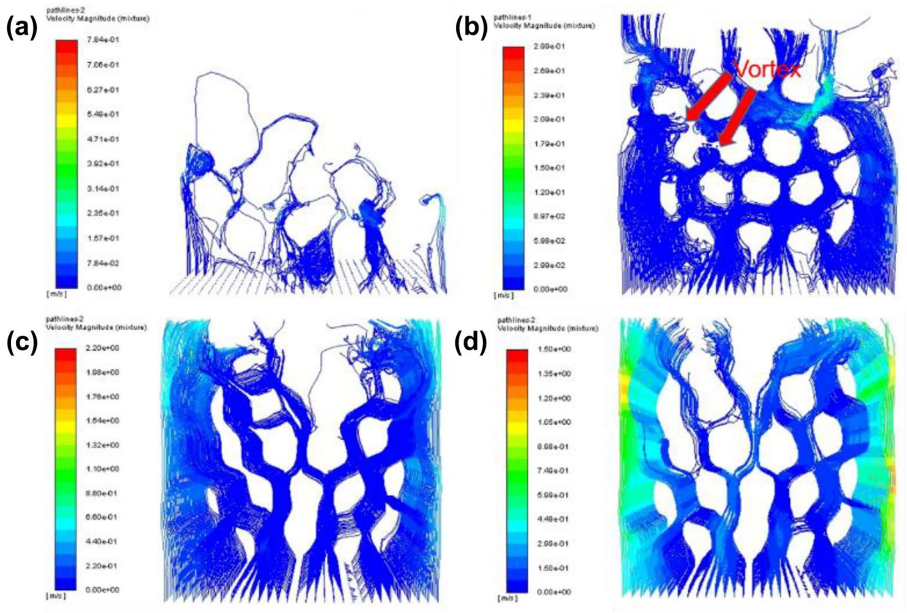

Fig. 15 Streamline of melt with different infiltration pressure: **a** 10kPa; **b** 100kPa; **c** 500kPa; **d** 1MPa

measured from Fig. 9a. With the surface tension range from 0.6~0.8 N/m, the infiltration pressure range from 2.28~3.06 MPa are required as calculated. The value agrees well with the numerical simulation result in the macroscopic scale, i.e., 3 MPa.

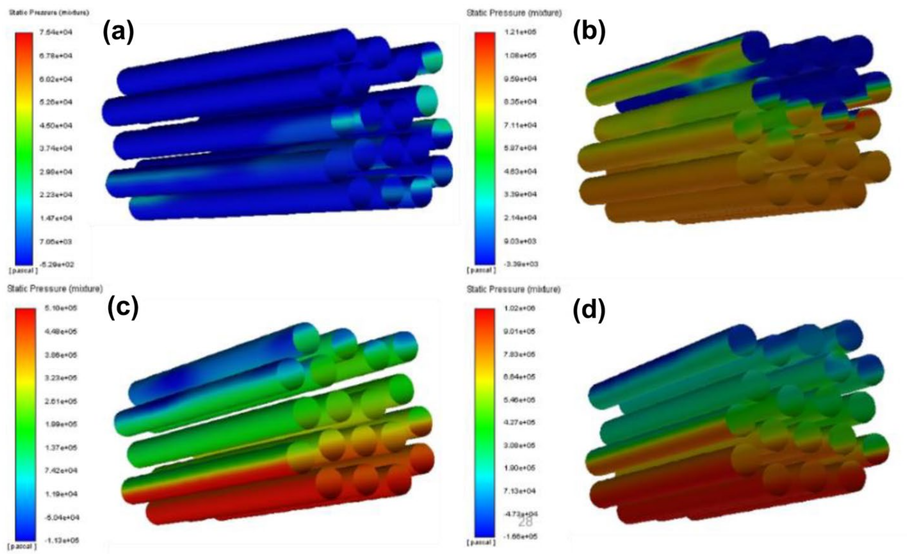

Fig. 16 Pressure distribution of melt with different infiltration pressure: **a** 10kPa; **b** 100kPa; **c** 500kPa; **d** 1MPa

Fig. 17 T-shaped CF/Al composite part

Table 5 presents the flow morphologies of intra-yarn. Results show that less infiltration time is required with the higher infiltration pressure exerted. Since the small capillary radius inside the yarn (usually several micros) leads to high resistance, there is no obvious difference in flow morphology with different infiltration pressure. With the lower infiltration pressure, the temperature of melt frontier decreases faster. With the infiltration pressure 10 kPa and 100 kPa, the melt cannot infiltrate the model completely. While with the infiltration pressure above 500 kPa, i.e., 0.5 MPa, the model can be fully infiltrated.

Figure 15 presents the streamlines in the intra-yarn with different infiltration pressures. It can be observed that with higher infiltration pressure, straight streamline of melt are obtained, which means high infiltration capacity. While with infiltration pressure of 10 kPa or 100 kPa, the streamlines are prone to be unsteady. Vortexes occur and might cause the void defects in the composites.

Figure 16 shows the pressure distributions with different infiltration pressures. The applied pressure drive the melt into the preform to form composite.

5 Experimental Results

T-shaped CF/Al composite part was produced by using the GPI process. According to the simulation results, the infiltration temperature was set to 720 ℃. The preheat temperature of graphite mold and preform was 550 ℃. The infiltration pressure as illustrated in Fig. 11 was exerted. T-shaped CF/Al composite part without defect was fabricated as showed in Fig. 17.

Figure 18 shows the SEM micrographs of the T-shaped CF/Al composite part in the transverse direction. It can be seen that the distribution of the fibers are homogeneous. There is no discernible void defect in the composite.

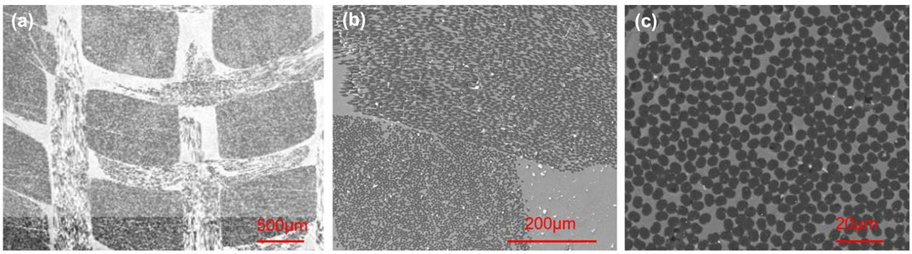

Fig. 18 SEM micrographs of T-shaped CF/Al composite

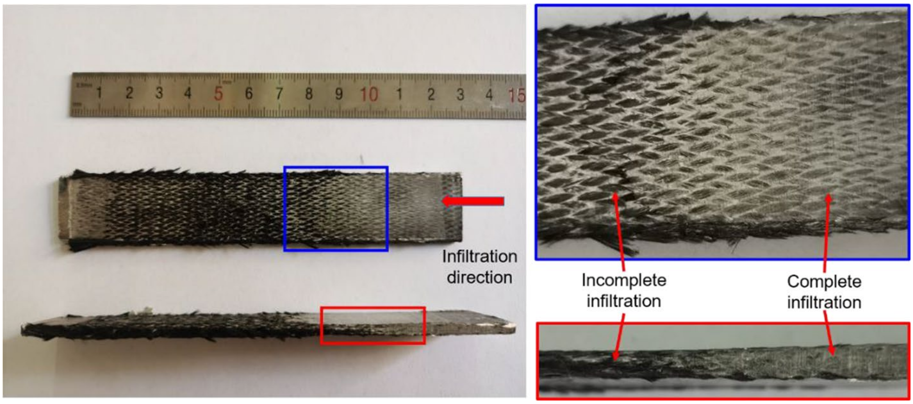

Fig. 19 CF/Al composite part with preheat temperature 450 ℃

The actual density (ρ_a) of the composite was determined using Archimedes's principle. The theoretical density (ρ_t) of the composite was calculated by the rule of mixture. Volume fraction of voids (V_v) can be calculated by using the following equation [38]:

$$V_v = \frac{\rho_t - \rho_a}{\rho_t} \times 100\% \tag{5}$$

Three specimens with the dimension of 10 mm×10 mm×3 mm were cut from the T-shaped CF/Al composite part. The actual density of each specimen was measured for three times to get the average, which is 2.104 g/cm^3. The theoretical density of the composite with the volume fraction of fabric 52% is calculated as 2.19 ± 0.1 g/cm^3. The volume fraction of voids is 3.93% by the Eq. 5. The conclusion can be drawn that high density CF/Al composite part can be obtained at the sufficient infiltration pressure and preheat temperature.

The flow simulation results indicates that the preheat temperature of fabric play a significant role in the infiltration process. Therefore, an additional experiment with the preheat

Fig. 20 SEM micrographs of CF/AL composite: **a**, **b** void defects among the yarns; **c**, **d** void defects inside the yarns

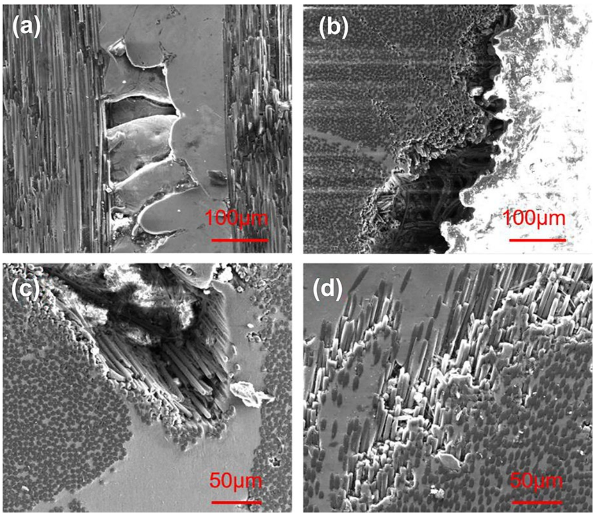

temperature of 450 ℃ was conducted. Plate fabrics with dimension of 130 mm×22 mm×3 mm were woven for further infiltration. The fabricated CF/Al composite parts are displayed in Fig. 19. Results show that the part away from the infiltration gate was incompletely infiltrated. Compared with the T-Shaped part in Fig. 17, the conclusion can be drawn that the preheat temperature of fabric should be set above the solidus of the matrix.

The SEM micrographs in Fig. 20 display the void defects in the CF/Al composite part, including the void in the inter-yarn (Fig. 20a and b) and intra-yarn (Fig. 20c and d). With the preheat temperature of preform below the solidus, the melt front lose its fluidity, resulting the formation of the voids.

6 Conclusions

1. The infiltration behaviors were successfully simulated by using the filter mode in ProCAST platform. The preheat temperature of fabric plays a key role in the fabrication of CF/Al composites by the GPI process. The preheat temperature should be set above the solidus to ensure the complete infiltration of the composites. The threshold infiltration pressure is around 3 MPa according to the simulation and experimental result.
2. With less flow resistance among the yarns, melt penetrates the interstices of inter-yarn firstly, then the internal fiber interstices of intra-yarn. Low infiltration pressure and preheat temperature might lead to the early solidification of the front melt, which will result in the void defects in the composite part.
3. With low infiltration pressure, the streamlines of melt in the intra-yarn tend to be unsteady. Vortexes occur and might cause the void defects in the composites.
4. The simulation in the macroscopic agrees well with the experimental result. While the simulation in the mesoscopic and microscopic scale were applied to explain the flow behaviors in the inter-yarn and intra-yarn, as well as the formation of the voids in the fabrication process of the CF/Al composites.

Acknowledgments This work was co-supported by the Education Department Project of Jiangxi Province (No. DA201903144), the National Natural Science Foundation of China (No.52165018); the Aeronautical Science Foundation of China (No. 2019ZF056013); and the Jiangxi Provincial Natural Science Foundation (No. 20202ACBL204010).

Data Availability Statements The datasets generated during and/or analyzed during the current study are available from the corresponding author on reasonable request.

Declarations

Conflict of interests The authors declare that they have no known competing financial interests or personal relationships that could have appeared to influence the work reported in this paper.

References

1. Hufenbach, W., Modler, N., Winkler, A.: Sensitivity analysis for the manufacturing of thermoplastic e-preforms for active textile reinforced thermoplastic composites. Procedia Materials Science **2**, 1–9 (2013). https://doi.org/10.1016/j.mspro.2013.02.001
2. Khosravani, M.R.: Composite materials manufacturing processes. Appl. Mech. Mater. **110–116**, 1361–1367 (2011). https://doi.org/10.4028/www.scientific.net/AMM.110-116.1361

3. Daoud, A.: Microstructure and tensile properties of 2014 Al alloy reinforced with continuous carbon fibers manufactured by gas pressure infiltration. Mater. Sci. Eng. A. **391**, 114–120 (2005). https://doi.org/10.1016/j.msea.2004.08.075
4. Hajjari, E., Divandari, M., Mirhabibi, A.R.: The effect of applied pressure on fracture surface and tensile properties of nickel coated continuous carbon fiber reinforced aluminum composites fabricated by squeeze casting. Mater. Des. **31**, 2381–2386 (2010). https://doi.org/10.1016/j.matdes.2009.11.067
5. Galyshev, S., Gomzin, A., Musin, F.: Aluminum matrix composite reinforced by carbon fibers. Materials Today: Proceedings. **11**, 281–285 (2019). https://doi.org/10.1016/j.matpr.2018.12.144
6. Zhu, C., Su, Y., Zhang, D., Ouyang, Q.: Effect of Al2O3 coating thickness on microstructural characterization and mechanical properties of continuous carbon fiber reinforced aluminum matrix composites. Mater. Sci. Eng. A. **793**, 139839 (2020). https://doi.org/10.1016/j.msea.2020.139839
7. Bhagat, R.B.: High pressure infiltration casting: manufacturing net shape composites with a unique interface. Mater. Sci. Eng. A. **144**, 243–251 (1991). https://doi.org/10.1016/10.1016/0921-5093(91)90231-B
8. Michau, V., Mortensen, A.: Infiltration processing of fibre reinforced composites: governing phenomena. Compos. Part. A. Appl. Sci. Manuf. **32**, 981–996 (2001). https://doi.org/10.1016/S1359-835X(01)00015-X
9. Bhagat, R.B., Amateau, M.F., Conway, J.C., Harbison, L.S.: SiC fiber reinforced aluminum matrix composites: high pressure squeeze casting and mechanical properties. Proc. 7th Int. Conf. on Composite Mater. 573-582 (1989)
10. Lee, H.S., Hong, S.H.: Pressure infiltration casting process and thermophysical properties of high volume fraction SiCp/Al metal matrix composites. Mater. Sci. Tech. **19**, 1057–1064 (2013). https://doi.org/10.1179/026708303225004396
11. Hufenbach, W.: Development of textile-reinforced carbon fibre aluminium composites manufactured with gas pressure infiltration methods. J Achiev Mater Manuf Eng **35**(2), 177–183 (2009). https://doi.org/10.1016/S0927-7757(00)00816-5
12. Lacost, E., Mantaux, O., Danis, M.: Numerical simulation of metal matrix composites and polymer matrix composites processing by infiltration: a review. Compos. Part. A. Appl. Sci. Manuf. **33**, 1605–1614 (2002). https://doi.org/10.1016/S1359-835X(02)00210-5
13. Lim, S.T., Lee, W.I.: An analysis of the three-dimensional resin-transfer mold filling process. Compos. Sci. Technol. **60**(7), 961–975 (2000). https://doi.org/10.1016/S0266-3538(99)00160-8
14. Lee, D.H., Lee, W.I., Kang, M.K.: Analysis and minimization of void formation during resin transfer molding process. Compos. Sci. Technol. **66**, 3281–3289 (2006)
15. Kang, M.K., Lee, W.I.: A dual-scale analysis of macroscopic resin flow in vacuum assisted resin transfer molding. Polym. Composite. **25**, 510–520 (2004). https://doi.org/10.1002/pc.20044
16. Gauvin, R., Trochu, F., Lemenn, Y., Diallo, L.: Permeability measurement and flow simulation through fiber reinforcement. Polym. Composite. **17**(1), 34–42 (1996). https://doi.org/10.1002/pc.10588
17. Dopler, T., Modaressi, A., Michaud, V.: Simulation of metal-matrix composite isothermal infiltration processing. Metall. Mater. Trans. B. **31**(2), 225–234 (2000). https://doi.org/10.1007/s11663-000-0041-z
18. Mantaux, O., Lacoste, E., Danis, M.: Numerical prediction of microporosity during the solidification of a pure metal within a porous preform. Compos. Sci. Technol. **62**, 1801–1809 (2002). https://doi.org/10.1016/S0266-3538(02)00081-7
19. Nie, M.M., Xu, Z.F., Yu, H., Wang, Z.J., Yao, J.: Effects of matrix alloy on fiber damage and fracture mechanism of continuous M40 graphite fiber/Al composites. Acta Materiae Compositae Sinica. **33**(12), 2797-2806 (2016). https://doi.org/10.13801/j.cnki.fhclxb.20160224.001
20. Park, C.H.: Numerical simulation of flow processes in composites manufacturing. Adv. Compos. Manuf. Proc. Des. 317-378 (2015). https://doi.org/10.1016/B978-1-78242-307-2.00015-4
21. Teng H.: An extension of Darcy's law to non-Stokes #ow in porous media. (2000)
22. Liu, Z.G., Wang, P.K.: Numerical investigation of viscous flow fields around multifiber filters. Aerosol. Sci. Tech. **25**, 375–391 (1996). https://doi.org/10.1080/02786829608965403
23. Forchheimer, P.: Wasserbewegung durch Boden. Zeitschrift des Vereins deutscher Ingenieure. **45**, 1781–1788 (1901)
24. Zeng, Z., Grigg, R.: A Criterion for non-Darcy flow in porous media. Transport in Porous Media **63**, 57–69 (2006). https://doi.org/10.1007/s11242-005-2720-3
25. Valdes-Parada, F.J., Ochoa-Tapia, J.A., Alvarez-Ramirez, J.: Validity of the permeability Carman-Kozeny equation: A volume averaging approach. Physica. A. **388**, 789–798 (2009)
26. ProCAST 2018.0 User's Guide, ESI Group

27. Bazhenov, V.E., Koltygin, A.V., Tselovalnik, Y.V., Sannikov, A.V.: Determination of interface heat transfer coefficient between aluminum casting and graphite mold. Russian Journal of Non-Ferrous Metals. **58**, 114–23 (2017)
28. Huchler, B.A.: Pressure Infiltration Behaviour and Properties of Aluminium Alloy-Oxide Ceramic Preform Composites. PhD Dissertation, The University of Birmingham, (2009)
29. Laurent, V., Chatain, D., Eustathopoulos, N.: Wettability of SiC by aluminium and AI-Si alloys. J. Mater. Sci. **22**, 244–50 (1987). https://doi.org/10.1007/BF01160579
30. Candan, E.: Effect of alloying elements to aluminium on the wettability of Al/SiC system. Turkish J. Eng. Env. Sci. **26**(1), 1–6 (2002)
31. Candan, E., Atkinson, H.V., Jones, H.: Effect of alloying additions on threshold pressure for infiltration and porosity of aluminium-based melt infiltrated silicon carbide powder compacts. Key Eng Mater **127–131**, 463–70 (1996). https://doi.org/10.4028/www.scientific.net/KEM.127-131.463
32. Iseki, T., Kameda, T., Maruyama, T.: Interfacial reactions between SiC and aluminium during joining. J. Mater. Sci. **19**, 1692–1698 (1984). https://doi.org/10.1007/BF00563067
33. Wang, Z., Wang, Z., Xiong, B., Cai, C., Xu, Z., Yu, H.: Micromechanics analysis on the microscopic damage mechanism and mechanical behavior of graphite fiber-reinforced aluminum composites under transverse tension loading. J. Alloys. and Compd. **815**, 152459 (2019). https://doi.org/10.1016/j.jallcom.2019.152459
34. Léger, A., Calderon, N.R., Charvet, R., Dufour, W., Bacciarini, C., Weber, L., Mortensen, A.: Capillarity in pressure infiltration: improvements in characterization of high-temperature systems. J. Mater. Sci. **47**, 8419–8430 (2012). https://doi.org/10.1007/s10853-012-6645-2
35. Ma, Y.Q., Zhao, Y.T., Zhang, Y., Wang, J., Chen, Y., Li, K.F., Ju, L.Y., Yu, Y.: Influence of infiltration pressure on the microstructure and properties of 2D-CFRP prepared by the vacuum infiltration hot pressing molding process. Polymers. **11**, 2014 (2019). https://doi.org/10.3390/polym11122014
36. Wang, Z., Gao, J., Chang, K., Meng, L., Zhang, N., Guo, Z.: Manufacturing of open-cell aluminum foams via infiltration casting in super-gravity fields and mechanical properties. RSC Advances. **8**, 15933–15939 (2018). https://doi.org/10.1039/C7RA13689G
37. Bainbridge, I.F., Taylor, J.A.: The surface tension of pure aluminum and aluminum alloys. Metall. Mater. Trans. A. **44**, 3901–3909 (2013). https://doi.org/10.1007/s11661-013-1696-9
38. Nanda, B.P., Satapathy, A.: Processing and characterization of epoxy composites reinforced with short human hair. Conference Series: Materials Science and Engineering, Iop Conference **178**, 012012 (2017). https://doi.org/10.1088/1757-899X/178/1/012012